Nanoscale

PAPER

View Article Online
View Journal | View Issue

Cite this: *Nanoscale*, 2023, **15**, 17793

Robust superhydrophobic silicone/epoxy functional coating with excellent chemical stability and self-cleaning ability†

Weidong Huang, [a,c] Xiaoli Jiang,[a] Yagang Zhang, *[a,c] Zhiqiang Tang,[a] Zicai Sun,*[b] Zhijun Liu,[b] Lin Zhao[a] and Yanxia Liu[a]

Superhydrophobic surfaces have attracted broad attention because of their unique water repellency but are restricted by poor wear resistance, weak adhesion to the substrate, and complex fabrication processes. Herein, a double-layer coating strategy consisting of the amino fluorine–silicone resin/epoxy resin (AFSR/EP) system is created. The system features a high hardness and transparent hydrophobic interface adhesive layer through the amine–epoxy "click" chemical reaction. The environmentally friendly resin system and low-cost nano-silica particles (n-SiO_2) are composited and sprayed onto the substrate surface to form a superhydrophobic layer with outstanding robustness and excellent environmental stability. The prepared AFSR/EP@n-SiO_2 composite coatings have a water contact angle of 161.1° and a sliding angle of 3.4°, demonstrating high superhydrophobic properties. Benefitting from the complementary advantages of silicone/epoxy resin, the prepared composite coatings maintain remarkable water repellency after various harsh environmental tests, including cyclic mechanical abrasion and tape-stripping, acid–base (pH 1 and pH 14) treatment, 10 wt% NaCl (pH 7) salt solution immersion, temperature treatment, knife scratching, and long-term ultraviolet radiation treatment, showing reinforced mechanical robustness and durable anti-corrosion stability. Notably, surface hardness of 5H and optical transparency over 80% can be achieved. The simple method offers a novel approach for the large-scale preparation of multifunctional superhydrophobic coatings.

Received 13th August 2023,
Accepted 22nd October 2023

DOI: 10.1039/d3nr04062c

rsc.li/nanoscale

1. Introduction

Coating is an important means of addressing functional surface defects in materials. Coatings can not only enhance the resistance to external damage of materials but also give the substrate more diverse, personalized, and functional demands, such as decorative effects like color, texture, and patterns,[1,2] and special requirements like electromagnetic shielding,[3,4] high-temperature resistance,[5] antifreeze,[6] and waterproofing.[7,8] Superhydrophobic coatings have attracted much attention due to their potential applications in solar-power devices,[9] metal corrosion,[10] and communication equipment.[11,12] The wettability of the object surface is determined by the surface chemical composition and the micro-geometry structure.[13,14] There is a scientific consensus that low surface energy materials combined with surface micro-nano structures can obtain superhydrophobic properties. Fluorinated resin is a kind of polymer material with special properties and high value.[15] Because fluorine atom has the characteristics of low polarizability, strong electronegativity, and small atomic radius, fluorine material has the properties of low surface energy and high stability. Fluorinated polymers containing C–F groups have excellent properties compared to other conventional polymers, such as no viscosity, low friction, and water resistance.[16,17] Recently, with the industrial upgrading of traditional industries and the vigorous development of emerging industries, fluorine polymers and fluorine resins have begun to be widely used in high-end equipment manufacturing, new energy, energy conservation and environmental protection, and other strategic fields.[18–20]

Silicone is a kind of material with excellent properties, such as low surface energy, high weather resistance, hydrophobicity, flame resistance, corrosion resistance, and non-toxicity.[21–23] Meanwhile, silicone resin is a polymer composed mainly of Si–O backbone structure and other special functional groups, such as methyl (–CH_3) and phenyl (–Ph), which are attached to the surplus bonds on Si atoms. It is precisely the unique in-

[a]*School of Materials and Energy, University of Electronic Science and Technology of China, Chengdu, 611731, China. E-mail: ygzhang@uestc.edu.cn, sunzic@mails.ucas.ac.cn*
[b]*Dongguan Yimei Material Technology Co., Ltd., Dongguan, 523000, China*
[c]*State Key Laboratory of Electronic Thin Films and Integrated Devices, University of Electronic Science and Technology of China, Chengdu 610054, China*
† Electronic supplementary information (ESI) available. See DOI: https://doi.org/10.1039/d3nr04062c

organic structure and the combined effect of functional groups that endow it with excellent physical and chemical stability. In general, the surface energy size of chemical groups is in the descending order of CH_2 < CH_3 < CF_3.[24] Therefore, many scholars utilize the low surface energy characteristics of organosilicon polymers to hydrophobically modify materials.[25] According to the reported studies on organic-silicon superhydrophobic coatings, the mainstream approach involves graft-modifying micro/nanofillers with PDMS,[6–8,26,27] long-chain siloxane hydrocarbons with high methyl content,[28,29] or perfluorinated siloxanes[30,31] with low surface energy. However, superhydrophobic coatings prepared by graft-modifying micro/nanofillers method mostly lack mechanical durability and resistance to harsh environments. Moreover, perfluorinated siloxanes are costly, and their high fluorine content is environmentally unfriendly.[32] Reasonable design of silicone resin structure can not only improve the comprehensive performance of superhydrophobic coatings but also reduce production costs. However, silicone resin has the disadvantage of poor bonding performance, so it is of great significance to improve the bonding performance of silicone and the material surface.

Epoxy resin possesses excellent adhesion, mechanical strength, and electrical insulation properties,[33,34] which have been widely used in coatings, adhesives, electronic packaging materials, and other fields.[34–36] But, due to the characteristics of its cross-linked network structure, it is brittle after curing,[37] and has poor withstanding stress cracking ability,[38] mediocre high temperature resistance, and weather resistance,[39] increasing the risk of many material applications. Hence, organic silicone materials and epoxy resins have strong complementary advantages in terms of performance. Specifically, the introduction of organic silicone segments in epoxy resins can not only fully reduce the surface energy of the material but also enhance its toughness, heat resistance, and water resistance. Importantly, the high adhesion, high structural strength, and airtightness of epoxy resins can be fully utilized, making it possible to prepare scratch-resistant superhydrophobic coatings. Due to the great distinction of molecular structure and solubility parameters modified by traditional physical blending,[40] the compatibility of polysiloxane and epoxy resin is poor, and phase separation and turbidity easily occur. On the contrary, chemical copolymerization modification can overcome such defects well.[41] Due to the modularity, stereospecificity, simplicity, and efficiency, the amine–epoxy "click" chemical reaction[42,43] has become a universal and powerful tool for the modification and functionalization of polymers.[43,44] By introducing flexible polysiloxane chain segments with large bond energy into the epoxy resin system, an interwoven network structure can be formed between the two materials, thus significantly improving the compatibility and reducing the size of the two phases. In addition, the flexibility of the epoxy resin, heat stability, flame retardancy, and hydrophobicity of the coating can be improved.

Most notably, due to the self-leveling characteristic of polymer resin in the liquid state, the roughness of the required surface micro-nano structure cannot be formed. Therefore, rigid nanoparticles are needed to provide a stable micro-nano structure skeleton. To meet the functional requirements of different fields, nanoparticles such as cerium dioxide (CeO_2),[11] titanium dioxide (TiO_2),[14,25] vanadium dioxide (VO_2),[26] and silicon dioxide (SiO_2)[7,8,45,46] are always applied to provide suitable surface micro-nanometer rough structures for the construction of superhydrophobic coatings. Among them, the production process of n-SiO_2 is highly mature, boasting not only low raw material costs but also the capability to meet extremely low particle size requirements ranging from 1 to 100 nm. n-SiO_2 has a large number of free hydroxyl groups on the surface, which can be dehydrated and condensed to form covalent bonds, thereby modifying various functional groups and making their surfaces extremely functional. Using low surface energy substances to modify the hydrophobic n-SiO_2 and then constructing a rough structure on the solid surface makes it a high-quality choice for the preparation of superhydrophobic coatings.

Along these lines, a highly transparent amino fluorine–silicone resin (AFSR) was synthesized using siloxane monomers to improve the compatibility between silicone resin and epoxy resin. By employing the amine–epoxy "click" chemical reaction, the physical and chemical stability, as well as the hydrophobicity of AFSR, were combined with the strong adhesion capability of epoxy resin, leading to the preparation of transparent and hydrophobic AFSR/EP coatings with excellent performance. With the assistance of rigid n-SiO_2, a superhydrophobic layer with abundant micro-nano hierarchical structures was further constructed on the AFSR/EP coating to form an AFSR/EP@n-SiO_2 double-layer composite coating. The AFSR/EP@n-SiO_2 coating exhibited dual outstanding properties inherited from silicone resin and epoxy resin, demonstrating remarkable stability, hydrophobicity, and self-cleaning ability. The robustness and hydrophobicity of the coating were analyzed from the mechanism. A series of tests were conducted to verify the durability of the coating, including sandpaper abrasion, tape peeling, immersion in acidic/alkaline/salt solutions, and exposure to ultraviolet light. The prepared hydrophobic/superhydrophobic gel can be directly sprayed onto various substrates, such as glass, steel, copper, and cardboard. The coating with superior practical operability fabricated *via* simple spraying methods and mild curing conditions makes large-scale preparation possible. This work provides a new insight into constructing superhydrophobic coatings with high wear resistance and stability.

2. Experimental

2.1. Materials

Modified polyfunctional group epoxy resin (T106 and T50, epoxy values of 1.06 mol per 100 g and 0.5 mol per 100 g, respectively) was obtained from Jiangsu Tetra New Material Technology Co., Ltd, China. Nano-silica particles (n-SiO_2) were received from Shanghai Keyan Industrial Co., Ltd. Furthermore, all other raw materials such as 1,3,5-tris (3,3,3-trifluoropropyl) methylcyclotrisiloxane (D3F), phenyltriethoxysilane (PTES) and *n*-(β-aminoethyl)-γ-aminopropylmethyl-

dimethoxysilane (KH-602), potassium hydroxide, toluene, xylenes, and anhydrous ethanol (EtOH), were purchased from Shanghai Macklin Biochemical Co., Ltd, China. Distilled water (DW) was produced in our lab. Glass slides (50 mm × 50 mm/30 mm × 100 mm surface area, 2 mm thick) were purchased from Luoyang Guluo Glass Co., Ltd, China. Other substrate materials are available in the market. The substrates were washed in ultrasonic cleaning agent and ethanol respectively and dried in oven before use.

2.2. Synthesis of amino fluorine–silicone resin (AFSR)

AFSR was synthesized through a one-pot method, as illustrated in Fig. S1 of the ESI.† Under nitrogen protection, PTES, KH-602, D3F, KOH, toluene, and DW were kept in a three-necked flask equipped with a thermometer, condenser, and an electric mixer, forming a solution and holding the hydrolysis reaction at room temperature for 30 min, and then the temperature was raised to 70 °C to continue the reaction for 8 h. Then, the reaction system was slowly heated to 120 °C to steam out the low-molecular-weight alcohols and excess water, and a transparent viscous polymer was obtained. After toluene was added to the polymer and diluted, 732 cation exchange resin was used to remove the strong alkali catalyst in the polymer, and the liquid obtained after filtration was vacuum distilled to 140 °C to remove toluene to obtain high transparency and purity AFSR. The theoretical amino active hydrogen value of the AFSR is 0.3 mol per 100 g.

2.3. Preparation of single-component resin solution

In order to ensure the cross-linking density of the curing system to the maximum extent, the ratio of the epoxy value of the EP to the active hydrogen value of the AFSR is about 1. 4.5 g of AFSR is dissolved in 15.5 g of mixed solvent (the mass ratio of xylene to ethanol is 2 : 3) and filtered through #300 gauze to form a transparent silicone resin solution. Similarly, 0.45 g of T50 and 1.05 g of T106 were melted to form a transparent liquid epoxy resin. After cooling to room temperature, 18.5 g of xylene was added and stirred to dissolve it, then filtered the mixture through #300 gauze to obtain a transparent epoxy resin solution. Each solution is a stable, transparent, and homogeneous system that will not undergo reactions or deterioration and can be stored for a long time.

2.4. Preparation of hydrophobic and transparent coatings and double-layer superhydrophobic coatings

Scheme 1 illustrates the construction strategies of hydrophobic and transparent coatings and double-layer superhydrophobic coatings. Firstly, the hydrophobic/superhydrophobic sol was prepared using the sol–gel method: 30 g of the above silicone resin and epoxy resin solution were separately taken in a 100 mL polythene bottle. 20 g of zirconia (ZrO_2, 2 mm in diameter) beads were added and mixed thoroughly for 30 min using a shaking machine. Then, the hydrophobic sol was filtered through #400 gauze and aged for 2 h. Similarly, by adding an appropriate amount of n-SiO_2 before mixing, superhydrophobic sol with different silica mass ratios could be prepared.

Secondly, to construct superhydrophobic surfaces on substrate materials, the above hydrophobic/superhydrophobic sol is evenly sprayed onto the substrate with a spray gun. The distance between the spray gun and the substrate should be kept at about 15 cm, and the spraying pressure should be 0.5 MPa.

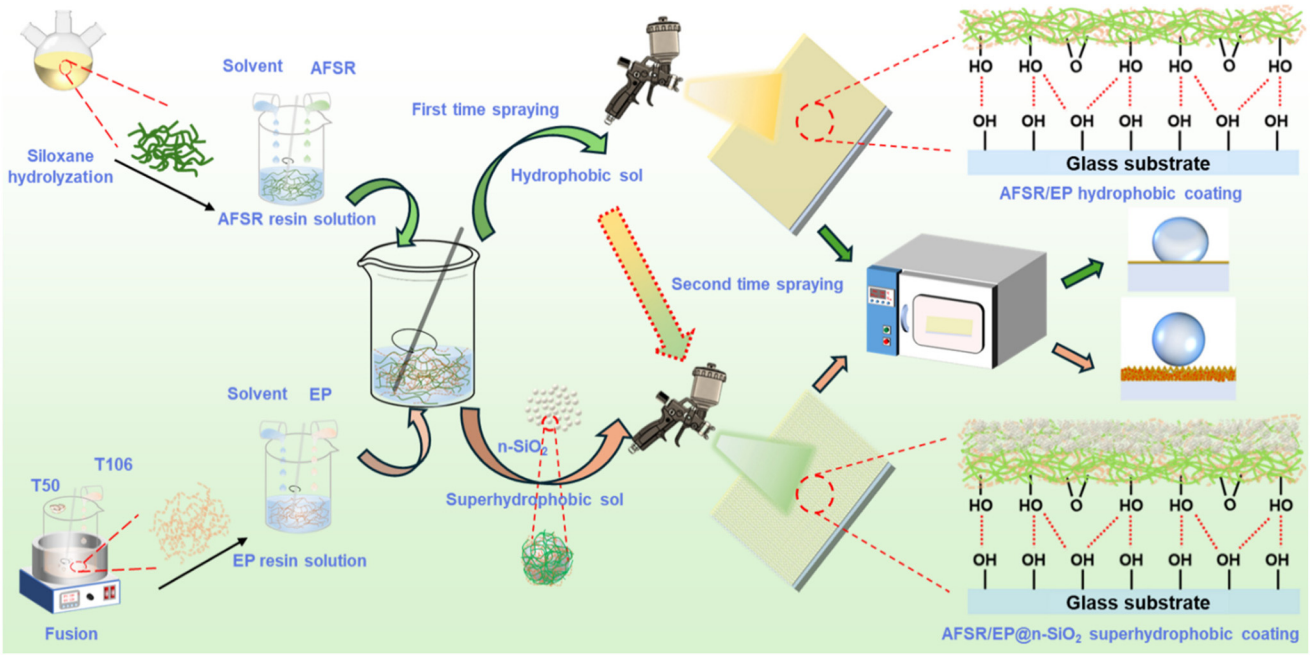

Scheme 1 The fabrication process of AFSR/EP hydrophobic coating and AFSR/EP@n-SiO_2 superhydrophobic coating.

The hydrophobic sol was sprayed 10 times in a back-and-forth cycle at a speed of 4 cm s^{-1} to form a hydrophobic coating. At the same time, the freshly sprayed hydrophobic coating was pre-cured for 10 min at 100 °C before being spray-coated with the superhydrophobic sol again 10 times in a back-and-forth cycle to form a superhydrophobic coating.

Finally, the transparent hydrophobic coating was obtained after curing for 2 h at 120 °C. It is worth noting that the prepared coating can be cured at room temperature for 24 h, but the hardness will be reduced.

For the convenience of differentiation, the coating with spray mass fractions of 0, 3, 4, 5, and 6% n-SiO_2 are defined as AFSR/EP-0, AFSR/EP-3, AFSR/EP-4, AFSR/EP-5, and AFSR/EP-6, respectively. The coated glass sample with the best overall performance, AFSR/EP-5, is also defined as AFSR/EP@n-SiO_2.

2.5. Characterization and testing

Surface morphologies and composition with a thin gold layer were observed using a Gemini SEM 360 field-emission scanning electron microscope (FE-SEM) equipped with an energy-dispersive X-ray spectrum (EDS) at an accelerating 10 keV under high vacuum. Furthermore, the structure of the synthesized polymer was characterized by an attenuated total reflection (ATR)–Fourier transform infrared (FTIR) analyzer (Bruker, INVENIO-R, Germany). The resolution of the ATR-FTIR spectra was 4 cm^{-1}, and the scanning range was 4000–400 cm^{-1}. ^{1}H nuclear magnetic resonance (^{1}H-NMR) spectra were carried out on an Avance NEO 600 (Bruker, Germany) at 500 MHz with $CDCl_3$ as a solvent and internal standard. X-ray photoelectron spectroscopy (XPS, Thermo Fisher ESCALAB XI+, USA) of the superhydrophobic coatings was conducted to analyse the composition and surface chemical states. The surface morphology and arithmetic mean roughness (R_a) of the coatings were investigated by atomic force microscopy (AFM, The Asylum Research Cypher S, UK). A Themys simultaneous thermal analyzer (TG-DSC, Setaram, France) was used to analyze the thermal stability of the synthesized polymer from 25 to 500 °C at rates of 10 °C min^{-1} in an O_2 environment. Transmittance measurements in the spectral range of 200–800 nm were conducted using an ultraviolet–visible (UV–vis) spectrophotometer (UH4150, HITACHI, Japan) and optical transparency was measured on a TH-100 haze meter. The water contact angles (CAs) were measured on a JC2000D2 optical contact angle measuring instrument at ambient temperature with a 5 μL water droplet, and the CA result was fetched from the average value of five measurements at different points of the sample. The bouncing behavior analysis of water droplets on the coating was further evaluated, and the volume of water droplets was 15 μL.

Mechanical damage and physiochemical stability test. The wear resistance of the coating was evaluated by a sandpaper (mesh number, #1000) wear test. The method was as follows: the sample was fixed on the test platform of the wear tester, and a load of 200 g was added. The static contact surface between the sandpaper and the coating was 1 cm × 1 cm below. Then, the load was used to reciprocate and wear the coating at a constant speed of 1 cm s^{-1} for 6 cycles per min. After every 5 cycles of wear, the contact angle and sliding angle of the coating were measured. The adhesion performance test of the coating to the substrate was evaluated using the standard Elcometer 99 tape test. After applying a weight of 500 g, the tape was peeled off from the substrate. The contact angle and sliding angle of the coating were measured after every 5 cycles of peeling. The chemical durability of the coating under extreme conditions was tested by measuring the contact angle (CA) and sliding angle (SA) of the coating after soaking in hydrochloric acid solution (pH = 1), potassium hydroxide solution (pH = 14), and 10 wt% NaCl solution (pH = 7) for specific time. For ultraviolet radiation damage, the prepared coating was treated with 30 W ultraviolet radiation for up to one month. During the temperature treatment, the coating was placed in a refrigerator (−20 °C) and on a heating test bench for 1 h, respectively, and then allowed to naturally recover to room temperature. The temperature of the heating test bench can be adjusted within the range from room temperature to 180 °C.

3. Results and discussion

3.1. Chemical structure design and curing mechanism of AFSR/EP

The supramolecular silicone resin of AFSR with low surface energy, high refractive index and transparency, and excellent compatibility with epoxy resin was synthesized by the hydrolysis and co-condensation reaction of PTES, KH-602, and D3F under the catalysis of potassium hydroxide (Fig. S1 in the ESI†). The amino functional groups were incorporated into the chemical structure as a reactive bonding point for epoxy groups. Meanwhile, the addition of the phenyl group improves the heat resistance of the material, and the fluorine group can further reduce the low surface energy of the silicone resin. To confirm the occurrence of the synthetic reactions, ATR-FTIR was carried out to compare the chemical structures of organic silicone monomer and AFSR. As shown in Fig. S2a of the ESI,† the peaks at 3361 cm^{-1}, 1599 cm^{-1}, and 3305 cm^{-1} were assigned to characteristic stretching vibrations of N–H.[7,47] The peaks at 3073 cm^{-1}, 1429 cm^{-1}, and 1262 cm^{-1} were ascribed to stretching vibrations of Ph–H, Ph–Si, and C–N bonds,[22,23] respectively. The peaks at 1071 cm^{-1} and 1006 cm^{-1} were attributed to the typical asymmetrical and symmetrical stretching vibrations of Si–O–C and Si–O–Si, implying the formation of silicon backbone structure.[48,49] The additional peak located at 1127 cm^{-1} was assigned to the stretching vibration of $-CF_3$ in D3F and AFSR molecules. The ^{1}H-NMR spectrum of the target supramolecular silicone resin was characterized. In the ^{1}H-NMR spectrum, the signals at around 7.5 ppm and 1.5 ppm correspond to the C–H and N–H in the phenyl and amino groups,[22] respectively. The signal at around 0.2 ppm is typically attributed to the C–H from the methyl group, and other positions are mainly attributed to C–H in different environments (Fig. S2b in ESI†). These results indicate that the AFSR has been synthesized successfully. The cross-linked vitrimer networks were prepared by amine–epoxy "click" chemical reaction

with modified epoxy resin (EP) and synthesized AFSR, which enabled desirable mechanical strength, high substrate binding, and high transparency properties. The product of the reaction between AFSR and EP, where the amino alcohols were generated *via* the reaction of epoxy with amino groups (Fig. 1a), is denoted as AFSR/EP. Fig. 1b shows the ATR-FTIR spectra of the reaction feedstock and the cross-linked vitrimer networks. At 904 cm^{-1} is the characteristic absorption peak of the epoxy group.[34] The modified multifunctional epoxy resin of T50 shows peaks of hydroxyl (–OH) and ether (C–O–C) bonds at 3452 cm^{-1} and 1072 cm^{-1}.[6,30] T106 belongs to the alicyclic group epoxy resin, and the strong peak at 1729 cm^{-1} is the characteristic peak of the stretching vibration of the carbonyl group in the ester bond.[50] The combination of the two epoxies provides the polymer with superior hardness, thereby increasing its resistance to mechanical damage. After reaction curing, although AFSR/EP has almost all the characteristic peaks of epoxy resin and silicone resin, the characteristic peaks of the amino group at 1599 cm^{-1} have disappeared significantly (Fig. 1b). This fully verified the occurrence of amine–epoxy "click" chemical reaction. Fig. 1c illustrates the TGA curves of EP, AFSR, and AFSR/EP polymer under oxygen atmosphere. For the pristine AFSR and EP, the initial degradation temperatures under a weight loss of 10% were 306.3 °C and 214.17 °C, respectively. At 500 °C, both AFSR and EP were almost completely decomposed with residual amounts of 5.63% and 0.44%, respectively, indicating that AFSR exhibited better thermal stability than EP due to its unique Si–O–Si skeleton structure. AFSR/EP exhibited two obvious weight loss regions, suggesting a two-stage degradation process. The initial degradation temperature of AFSR/EP was 337.3 °C, yet the residual amount at 500 °C was 24.57%, demonstrating that the interpenetrating cross-linked polymer network structure improved the thermal resistance of the AFSR/EP system, effectively overcoming the poor thermal stability of the pure epoxy resin. The compatibility of superhydrophobic materials is an important factor of material properties, which will directly affect the application value and stability of materials.[40,41] Fig. S3 of the ESI† illustrates the visual changes of AFSR and EP before and after cross-linking and curing reactions, indicating that the sample has undergone a transformation from a homogeneous mixture before the reaction to a cross-linked and cured polymer during the reaction. The excellent transparency also confirms the high compatibility between AFSR and EP, providing feasibility for the preparation of transparent coatings (Fig. S3b in the ESI†).

3.2. Surface morphology and composition of AFSR/EP@n-SiO_2 coating

The superhydrophobic paint was prepared by simply mixing AFSR solution, EP solution, and n-SiO_2, which could be applied on various substrates *via* the facile spraying method.

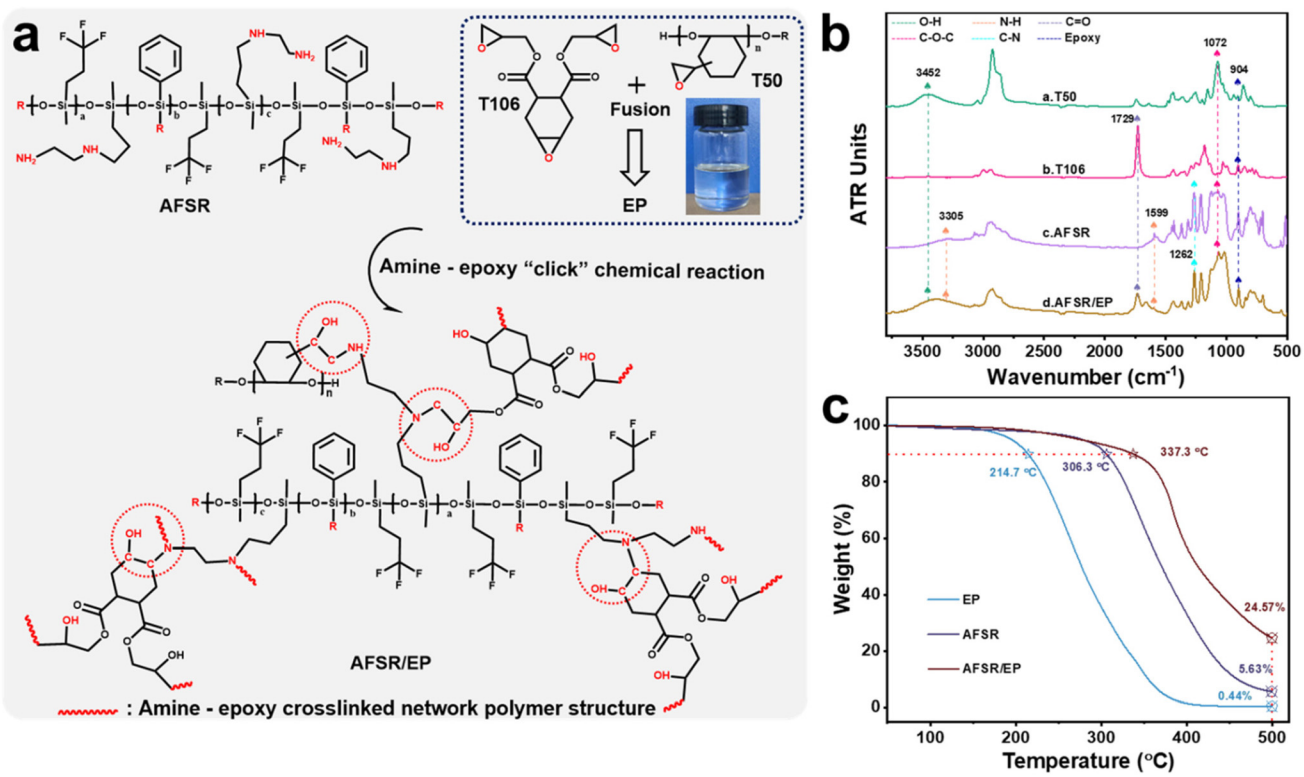

Fig. 1 The chemical structure design of supramolecular silicone polymer. (a) Amino–epoxy "click" chemical reaction process and chemical structure, inset of (a) is an image of the mixture of T106 and T50, which has good transparency properties. (b) The ATR-FTIR spectra of modified polyfunctional group epoxy resin T50 and T106, self-synthesized amino fluor silicone resin AFSR, and supramolecular silicone polymer AFSR/EP. (c) TGA curves of EP, AFSR and AFSR/EP.

Fig. S4 of the ESI† shows the SEM images of the sample coating structure at the scale of 100 μm, which indicates that the coating is uniformly attached to the substrate. When AFSR/EP hydrophobic sol was sprayed on a glass plate, a transparent and hydrophobic coating was formed with a CA of about 117.7° (Fig. 2a), which is larger than that of the pure glass surface of 35.15° (Fig. S5a in ESI†), suggesting the highly hydrophobic nature of AFSR. As clearly depicted in Fig. S5b of the ESI,† in the visible range (300–800 nm), the transmittance of uncoated glass is about 90%, which is only slightly reduced. In the illustration, although the picture of the plant under the coated glass appears unclear due to the uneven coating, it does not affect the effect of transparency. This makes it possible for the hydrophobic application of the coating in the optical field.[51,52] Obviously, although the low surface energy polymer can show a better hydrophobic effect, the structure without micro and nano rough is still unable to achieve the superhydrophobic performance requirements. To further improve hydrophobicity, n-SiO_2 is blended with polymers to improve the surface micro-nano structure. As shown in Fig. 2e, when the loading capacity of n-SiO_2 is 3 wt%, the CA of the AFSR/EP-3 coating is only 115.6°, which is slightly lower than that of AFSR/EP-0. This is because the resin completely covers the nanoparticles and prevents the formation of micron/nanometer coarse superstructures (Fig. 2b). As shown in Fig. 2c and d, the surface micro-nano structure morphology of the coating becomes more abundant and uniform with the loading of n-SiO_2 increased to 4% and 5% wt%. When the loading was 4 wt%, agglomeration of nanoparticles could be observed, resulting in incomplete coverage of the bonding layer and uneven distribution of micron and nanometer rough structures with a CA of 137°. For the AFSR/EP-4 coating, despite the agglomeration of nanoparticles, the polymer honeycomb structure can still be observed on the surface of the coating. Due to the combination of low surface energy AFSR and micron-nanometer rough structure, the CA of AFSR/EP@n-SiO_2 coating

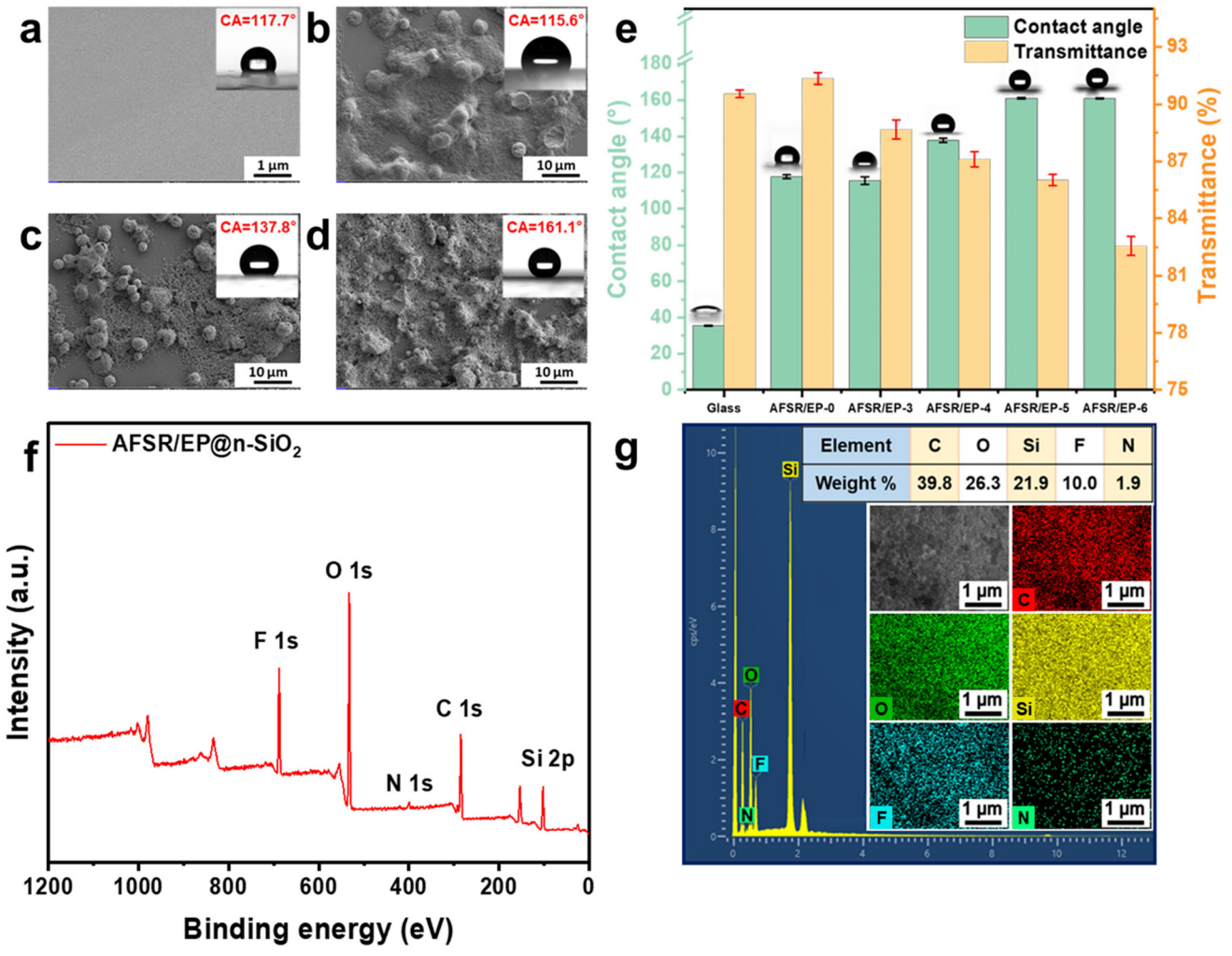

Fig. 2 FE-SEM images of AFSR/EP@n-SiO_2 coatings with different contents of n-SiO_2 particles and the corresponding surface wettability, (a) n-SiO_2 = 0 wt%, (b) n-SiO_2 = 3 wt%, (c) n-SiO_2 = 4 wt%, and (d) 5 wt%, respectively. (e) Hydrophobicity and transparency of coatings with different n-SiO_2 contents. (f) XPS spectra for AFSR/EP@n-SiO_2 superhydrophobic coating glass sheet substrate. (g) EDS spectrum of AFSR/EP@n-SiO_2 and corresponding mapping images of C, O, Si, F, and N elements.

with 5 wt% of n-SiO_2 is up to 161.1°, exhibiting typical superhydrophobicity. The static contact angle and the test results of the haze meter on the transmittance of AFSR/EP@n-SiO_2 coatings with different nanoparticle loads are shown in Fig. 2e. It is worth noting that the optical transmittance of the pure glass is about 90.56%, while the optical transmittance of AFSR/EP coated glass is about 91.35%. This is due to the high refractive index of the designed AFSR, which can improve the optical transmittance. Although the optical transmittance of the AFSR/EP@n-SiO_2 coating gradually decreased with the increase in nanoparticle loading, the coating still maintained a transmittance of 82.56% when the nanoparticle loading was 6 wt%. The result implies that the coating has good optical properties and can meet the corresponding transmittance requirements for applications. As can be seen from Fig. 2e, when the nanoparticle loading is 5 wt%, the hydrophobic properties of the coating reach a saturated state. The hydrophobicity of the coating could not be improved effectively by the addition of excessive nanoparticles. Instead, it will greatly reduce the transparency of the coating. Considering the hydrophobic performance and transparency exhibited by the surface micro-nano morphology distribution combined with coatings, the spray-coated superhydrophobic AFSR/EP-5 coating (AFSR/EP@n-SiO_2) with 5 wt% of SiO_2 was the optimal material. Therefore, in the subsequent sections, unless otherwise specified, all further performance tests were conducted using the AFSR/EP@n-SiO_2 coating.

The surface chemical composition of the AFSR/EP@n-SiO_2 coating was confirmed by X-ray photoelectron spectroscopy (XPS) and energy dispersive X-ray spectrometer (EDS). As shown in Fig. 2f, the XPS spectrum of the AFSR/EP@n-SiO_2 coating shows peaks at 532.7 eV, 400.3 eV, 284.7 eV, and 101.0 eV, corresponding to O 1s, N 1s, C 1s, and Si 2p,[31,53] respectively. Typical F 1s peaks appear at around 688.6 eV, which can be assigned to trifluoromethyl.[49,54] As shown in the SEM-EDS spectra (Fig. 2g), the AFSR/EP@n-SiO_2 coating presents a uniform distribution of elements C, O, Si, F, and N, with atomic percentages of 39.28, 26.3, 21.9, 10.0, and 1.9%, respectively, indicating the uniform modification of coating on the substrate. Furthermore, the F elements derived from trifluoromethyl of D3F are low-surface-energy groups for enhancing surface water repellency. The above results indicate that the surface layer of the coating meets the condition of low surface energy, which is conducive to the formation of the superhydrophobic coating.

The surface topography and surface roughness changes of AFSR/EP@n-SiO_2 coatings were further investigated by AFM (Fig. 3). In the high-mode image, the AFSR/EP-0 hydrophobic

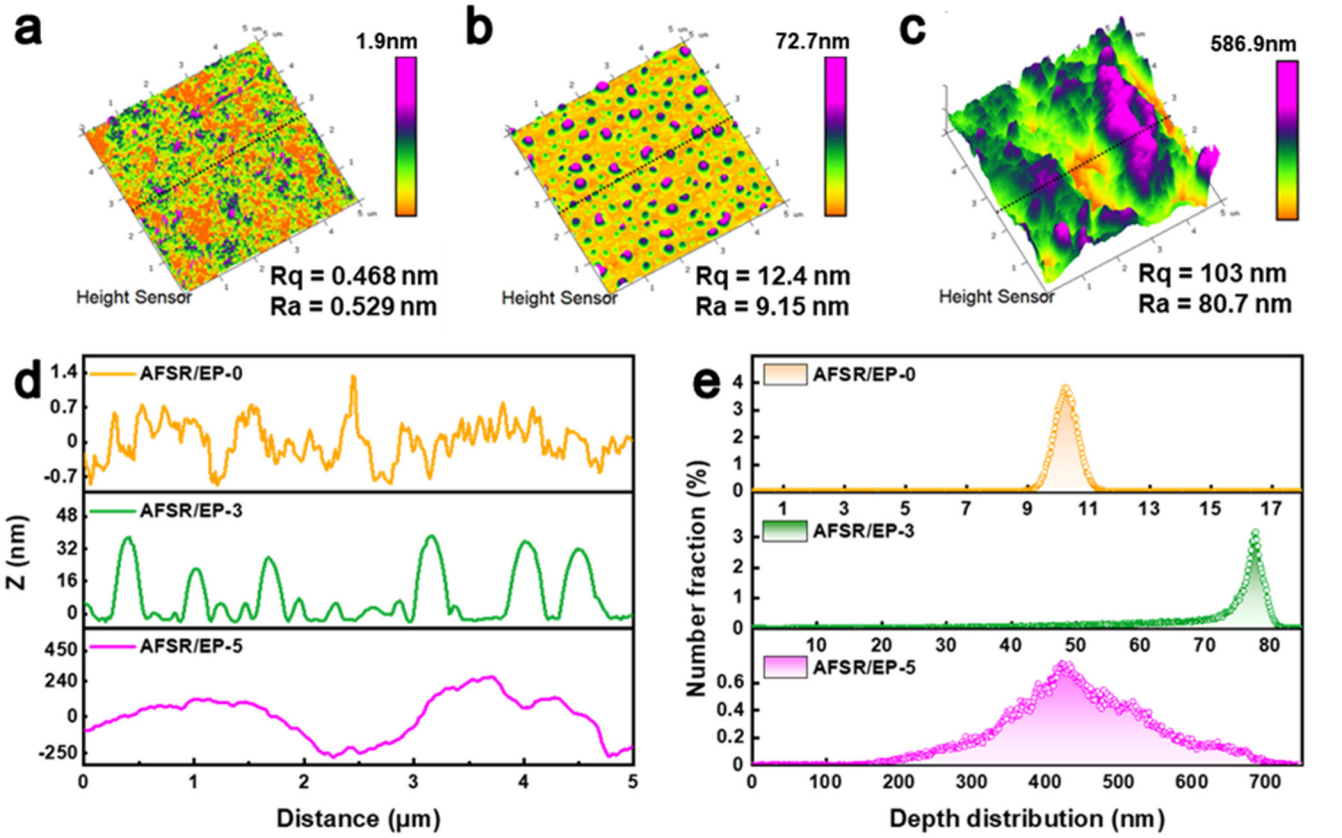

Fig. 3 Height-mode AFM images (scan area of 5 × 5 μm^2) of AFSR/EP@n-SiO_2 coatings with different contents of n-SiO_2 particles, (a) n-SiO_2 = 0 wt%, (b) n-SiO_2 = 3 wt%, and (c) 5 wt%, respectively. (d) AFM 3D images showing the cross-sectional micro profiles at 2.5 μm of the AFSR/EP@n-SiO_2 coating. (e) Statistical distribution of the height of the coating on the glass sheet substrate.

coating presents a relatively uniform and smooth nano-morphology, and its surface average coarse roughness (R_q) value is only 0.468 nm and root mean square roughness (R_a) value is 0.329 nm (Fig. 3a). When the nanoparticle content increases to 3 wt%, the R_q value of AFSR/EP-3 coating is 12.4 nm and the R_a value is 9.15 nm (Fig. 3b), suggesting a remarkable increase of surface roughness. As shown in Fig. 3c, the superhydrophobic AFSR/EP-5 exhibits the highest R_q (103 nm) and R_a (80.7 nm) values, indicating reasonable nanoparticle addition could optimize the surface topography. Fig. 3d shows the cross-section microscopic profile of the AFSR/EP@n-SiO_2 coating at 2.5 μm. The agglomeration of nanoparticles resulted in an obvious fluctuation of the curve, and the depth between the wave ridge on each coating surface and the cave was 0–1.4 nm, 0–40 nm, and 0–500 nm, respectively. The surface height distribution of the 5 × 5 μm area increased with the increase in nanoparticle content. Specifically, the main height distribution range changed from 9–10 nm for AFSR/EP-0 to 70–80 nm for AFSR/EP-3, and then to 200–700 nm for AFSR/EP-5 (Fig. 3e). These results strongly demonstrate the importance of micron and nanometer rough structure for the superhydrophobic properties of the coating.

3.3. Structure design and hydrophobic mechanism of coating

The strong bonding property between coating and substrate is an indispensable and important index in the research of superhydrophobic coating materials. The cross-sectional image of the coating is shown in Fig. 4a. The thickness of the hydrophobic adhesive layer AFSR/EP and the superhydrophobic surface layer AFSR/EP@n-SiO_2 are both between 3 and 4 μm. Even with two-step spraying, the interface is still tightly bonded and void-free, which could be attributed to the excellent compatibility of AFSR and EP resins. In addition, the image also shows the excellent adhesive effect between the cross-linked polymer network and the substrate. Fig. 4c illustrates the schematic diagram of the coating structure and the adhesive mechanism between the coating and the substrate. First, AFSR/EP composite resin will penetrate into the gap or convex of the substrate, and after curing, a meshing force is generated in the interface area, which is a physical mechanical force.[55] Second, there is an electron acceptor-donor combination between the AFSR/EP composite resin and the substrate.[56,57] In the adhesion process between the substrate and the resin, there are a large number of electron-accepting groups (alkyl, phenyl, and halogen atoms) in the resin and corresponding electron-donating groups (hydroxyl, oxygen anions, and metal ions) on the substrate. At this time, electrons will transfer from the donor (substrate) to the acceptor (polymer), which forms a double electric layer on both sides of the interface region, resulting in an electromagnetic adsorption force. Third, chemical bonding is often a decisive factor in the adhesion performance of the coating.[33,34] AFSR/EP cross-inked polymer network has many active groups (such as unreacted amino, epoxy, and hydroxyl), which can form chemical bonds with hydroxyl groups on the substrate surface, hydrogen bonds, and van der Waals forces.[58] Therefore, under

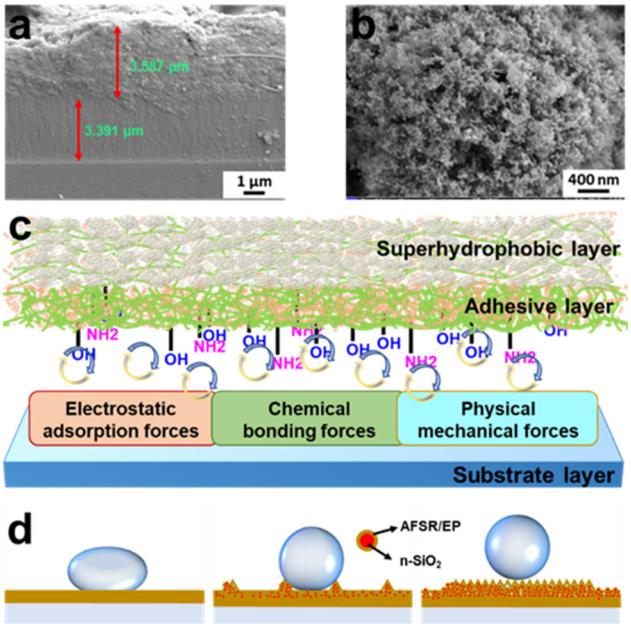

Fig. 4 (a) FE-SEM image of double-layer cross-section surface of glass sample with coating. (b) High power FE-SEM image of the AFSR/EP@n-SiO_2 superhydrophobic coating surface at nanoscale magnifications. (c) Schematic diagram of the layered structure of the AFSR/EP@n-SiO_2 superhydrophobic coating and the mechanism of strong bonding properties, and (d) simplified wetting model of three rough coating structures and different hydrophobic mechanism diagrams.

the combined action of a variety of forces, the coating and the substrate have excellent bonding properties, which will be verified later.

It is well known that the nanostructure of coatings plays a critical role in the superhydrophobicity of coatings. Fig. 4b and Fig. S6 of the ESI† show the morphological states of the coatings at the same nanoscale, revealing a mesh structure formed by spherical n-SiO_2 and cross-linked polymer network. As shown in Fig. S6a of the ESI,† the AFSR/EP coating exhibits a surface morphology resembling shattered glass due to the curing shrinkage of AFSR/EP. The addition of n-SiO_2 prevents the shrinkage of the cross-linked polymer network (Fig. S6b and c of the ESI†), making the three-dimensional mesh structure more abundant and greatly enhancing the hydrophobicity of the coating. Furthermore, we have developed wetting models of the coating structures on substrates with different roughness using simplified diagrams (Fig. 4d). The cross-linked polymer network of AFSR/EP only satisfies the single condition of low surface energy. Therefore, it cannot achieve the superhydrophobic effect. With a small number of added nanoparticles, the hydrophobicity of the coating is improved with the increase in surface roughness. However, the spray process would aggravate the aggregation of nanoparticles, making it difficult to form the mesh structure, which greatly hinders the rolling of droplets. Therefore, with a further increase of nanoparticles, the surface structure of the coating gradually conforms to the Cassie–Baxter wetting model.[8] The existence of the mesh structure prevents air stored in the gaps

from being expelled by droplets, resulting in the inability to wet. The reduction in the contact area of the solid surface weakens the adhesion force of droplets, leading to the increase of CA and the decrease of sliding angle (SA). In the microstructure of the coating, the contact area between the droplet and the material is reduced by adding n-SiO_2 to improve the coarse overshoot, and the repulsion of the coating on the droplet is increased by low surface energy resin. The combined effect of the two guarantees the excellent superhydrophobic characteristics of the AFSR/EP@n-SiO_2 coating.

3.4. Robustness, durability, and stability of coating

Two strips of glass were bonded and cured by AFSR/EP resin with a contact area of 3 cm^2 by the Lap-shear bonding strength test. According to the ISO 4587 standard, the binding strength of AFSR/EP is 7.4 ± 0.5 MPa, indicating good interfacial reliability between the bonding layer and the substrate. The poor mechanical stability of superhydrophobic surfaces is a crucial factor limiting their widespread application in industry. The micro-nano rough structure of superhydrophobic surfaces is prone to damage, resulting in a reduction in their performance due to mechanical wear and tear. To demonstrate their mechanical robustness, various methods were employed to evaluate the mechanical durability of the AFSR/EP@n-SiO_2 coating. First, a wear testing machine was used to systematically test the resistance of the superhydrophobic coating to mechanical abrasion. As shown in Fig. 5a, the AFSR/EP@n-SiO_2 coating was fixed to a wear testing station and loaded with a weight of 200 g. The sandpaper on the coating surface was moved back and forth for one cycle, with a wear distance of 10 cm. Images of the coating after 0, 15, and 100 cycles of wear are shown in the insets Fig. 5a. After 100 cycles of wear, the coating has been severely broken to expose the substrate. Although sandpaper wear will cause n-SiO_2 to fall off and the surface micro-nano structure to be broken, the coating can still maintain superhydrophobic properties under certain wear degrees. As shown in Fig. 5b, the CA gradually decreases, and the sliding angle gradually increases with the increase of wear cycles. Compared with some reported wear-resistant superhydrophobic surfaces,[28,59,60] the AFSR/EP@n-SiO_2 coating remained superhydrophobic after 25 cycles of wear (250 cm) under a load of 200 g (CA: 152.6°, SA: 9.6°). This can be attributed to the organic silicone epoxy cross-linked polymer network, which possesses good adhesion and wear resistance. In addition, the surface hardness of the composite coating was determined using the pencil hardness test. The schematic diagram of the coating hardness testing device is shown in Fig. 5d. The test results, according to ASTM D3363 standard, indicate that the surface hardness of the coating is 5H. Although mechanical wear can damage the surface rough structure, the presence of nanoparticles ensures that the wear does not have a significant impact on the surface roughness of

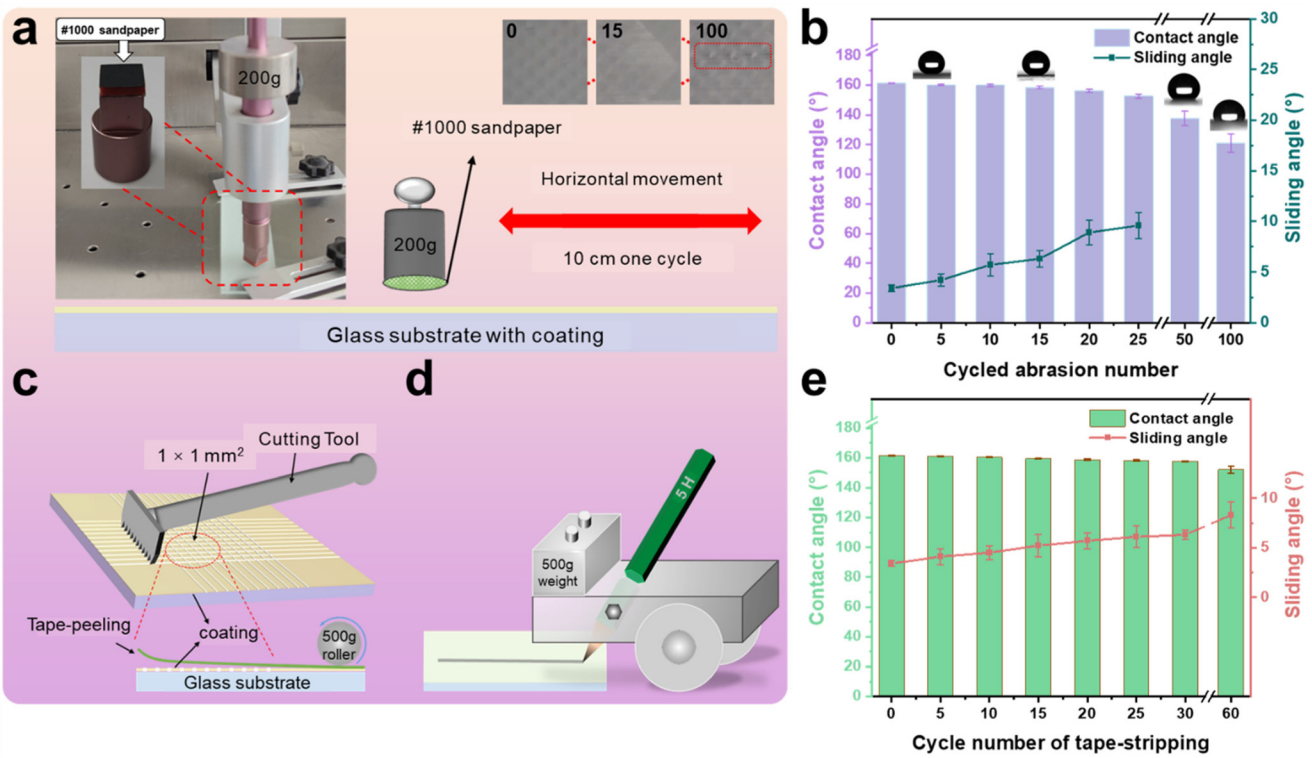

Fig. 5 Mechanical robustness of the composite coatings. (a) The schematic of the abrasion test for AFSR/EP@n-SiO_2 superhydrophobic coatings. The insets show the corresponding wear state with corresponding cycle images of 0, 15, and 100. (b) Changes of contact angle and sliding angle with different cycles of abrasion. (c) Schematic diagram of cycle of tape-stripping test and ASTM-D3359 adhesion test. (d) The schematics of the device for ASTM-D3363 testing the hardness of the coating. (e) Changes of CA and SA with different cycles of tape-stripping.

the coating, which is critical for maintaining superhydrophobicity. With the increase of wear cycles, the detached nanoparticles further act as abrasives, causing deep wear in certain areas of the coating, resulting in a significant decrease in hydrophobicity and loss of sliding angle. After 50 cycles of wear, the coating lost its rolling ability (CA: 137.7°).

Good adhesion is crucial for coatings. As shown in the schematic diagram in Fig. 5c, the adhesion of the coating was tested using a coating adhesion tester. According to the ASTM D3359 standard, the bond strength reached 5B. After the AFSR/EP@n-SiO_2 coating was tested, the cut edge was completely smooth, without any visible peeling traces, showing good tape peeling resistance (Fig. S7 in the ESI†). In tape peeling tests (Fig. 5e), the coating surface maintained its hydrophobicity (CA: 152.0°, SA: 8.3°) even after 60 peelings. The tape peeling test demonstrated that the cross-linked polymer network encapsulates the nanoparticles, allowing them to be fully incorporated into the mesh structure, thereby preventing their detachment. Furthermore, as shown in the video Movie S1 of the ESI,† the coating sample is subjected to repeated scratch damage experiments with a sharp blade. Although several scratches have been produced on the surface of the coating, there is no effect on the superhydrophobic properties of the AFSR/EP@n-SiO_2 coating sample.

Superhydrophobic coatings require excellent chemical stability and resistance to UV irradiation for various harsh environments. To verify the excellent performance stability of the AFSR/EP@n-SiO_2 coating, glass samples coated with the material were immersed separately in a strongly acidic solution (HCl, pH = 1), strongly alkaline solution (KOH, pH = 14), and high-concentration salt solution (NaCl, pH = 7, 10 wt%), and were also placed in a UV light test box (30 W). The changes in CA and SA of the AFSR/EP@n-SiO_2 coating were tested at different treatment times to evaluate the chemical stability and UV radiation resistance of the coating under extreme conditions, as shown in Fig. 6. It can be seen that the AFSR/EP@n-SiO_2 coating had excellent superhydrophobic performance (CA ≈ 161.1°, SA ≈ 3.4°) before any treatment. After

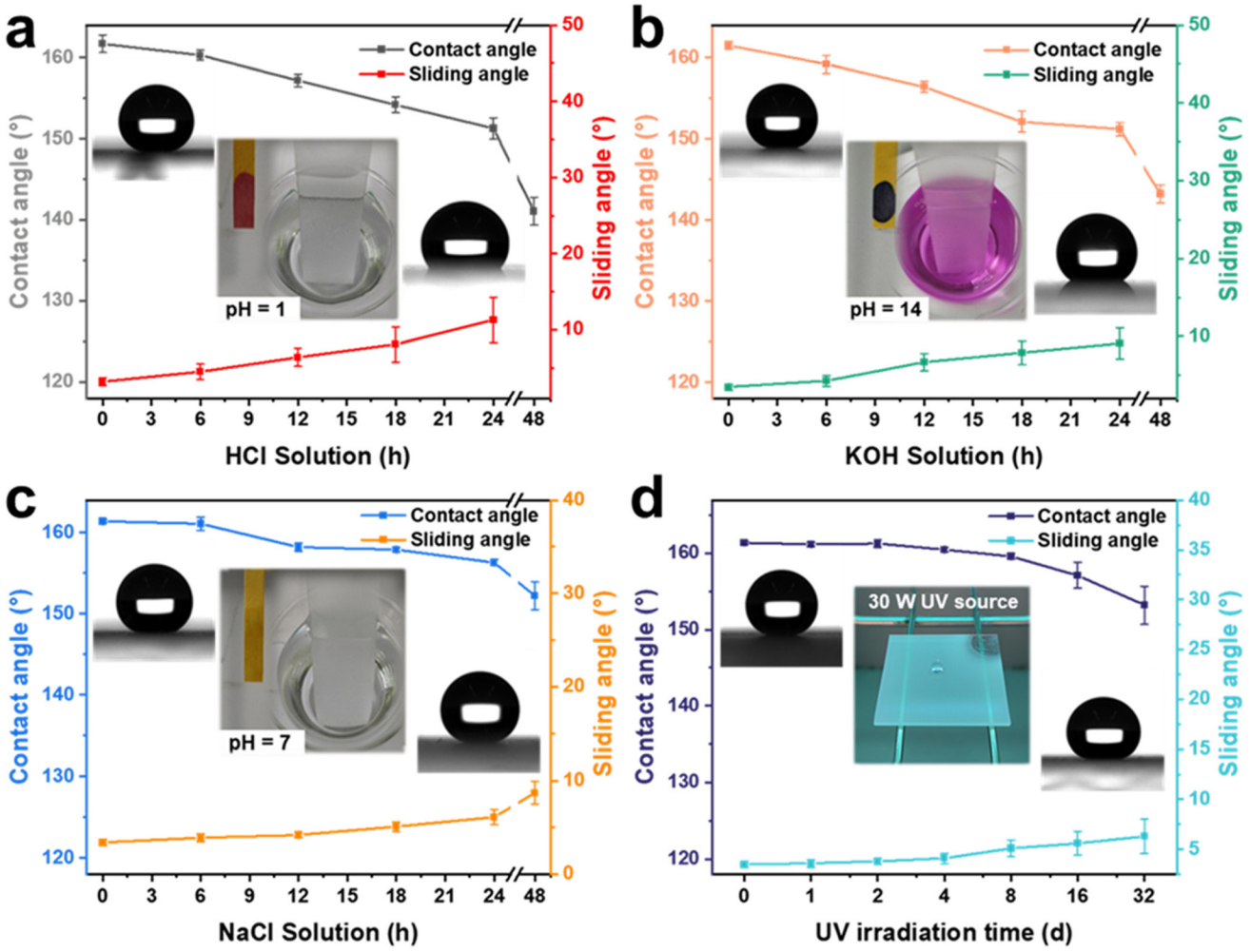

Fig. 6 Contact angle and sliding angle of AFSR/EP@n-SiO_2 coatings immersed in various harsh solutions with (a) pH = 1, HCl, (b) pH = 14, KOH, phenolphthalein indicator was added for color indication, and (c) pH = 7, NaCl (10 wt%) for a long time. (d) Hydrophobicity test of the prepared surface under 30 W ultraviolet light source.

immersion in the strongly acidic solution for 24 h, the CA was 151.3 ± 1.3° and the SA was 11.3 ± 3°. After 48 h of immersion, the coating had completely lost its superhydrophobic properties, and the CA was only 141.3 ± 1.7°, with no rolling ability (Fig. 6a). Similarly, after immersion in a strongly alkaline solution for 24 h, the CA was 151.2 ± 0.8°, and the SA was 9.1 ± 2°. After 48 h of immersion, the coating also lost its superhydrophobic properties, and the CA was only 143.2 ± 1.1°, with no rolling ability (Fig. 6b). After 48 h of immersion in a high-concentration salt solution environment, the coating maintained its superhydrophobicity, with a CA of 152.2 ± 1.7° and a SA of 8.7 ± 1.2° (Fig. 6c). This indicates that the prepared AFSR/EP@n-SiO_2 coating has better durability in extreme chemical solution environments than has been reported.[6,28,61,62] The excellent corrosion resistance is mainly attributed to the double-layered design and micro-nano-rough surface structure of the coating, which provides stable chemical bonds in the silicon oxide chain to effectively resist the corrosion of various chemical substances. The mechanism of ion corrosion resistance can be explained as follows: when the corrosive liquid contacts the coating, the micro-nano-layered structure captures a large amount of air to form air holes on the coating surface. These air holes can effectively prevent the diffusion of corrosive medium ions on the coating surface, thus providing an isolation and protective barrier between the corrosive medium and the surface (Fig. S8 in ESI†). From Fig. 6d, it can be seen that the AFSR/EP@n-SiO_2 coating still maintains its superhydrophobic properties (CA: 153.2 ± 2.5°, SA: 6.3 ± 1.7°) after long-term UV radiation exposure for 32 days. In addition, the AFSR/EP@n-SiO_2 coating retains satisfactory water resistance after being treated at different temperatures (*i.e.*, −20 °C–180 °C) (Fig. S9 in the ESI†). The above experimental results fully confirm the excellent physical and chemical stability of the AFSR/EP@n-SiO_2 coating.

As shown in Table S1,† there are also other reports on superhydrophobic coatings.[64–67] Compared with these previously reported results, the prepared AFSR/EP@n-SiO_2 coatings in this work exhibited high overall performance in all stability tests, fully demonstrating the excellent properties of the coatings.

3.5. Dynamic analysis of bouncing behaviour and non-stacking characteristics

To investigate the bouncing dynamics of water droplets on the super-hydrophobic coating of AFSR/EP@n-SiO_2, drop impact experiments (15 μL) were carried out on the coating.[63] As shown in Fig. 7a and Movie S2 of the ESI,† the impact process of the droplet on the superhydrophobic coating can be roughly divided into three stages: expansion, contraction, and complete rebound. Due to abundant air pockets on the coating surface, the droplet experiences a complete rebound immedi-

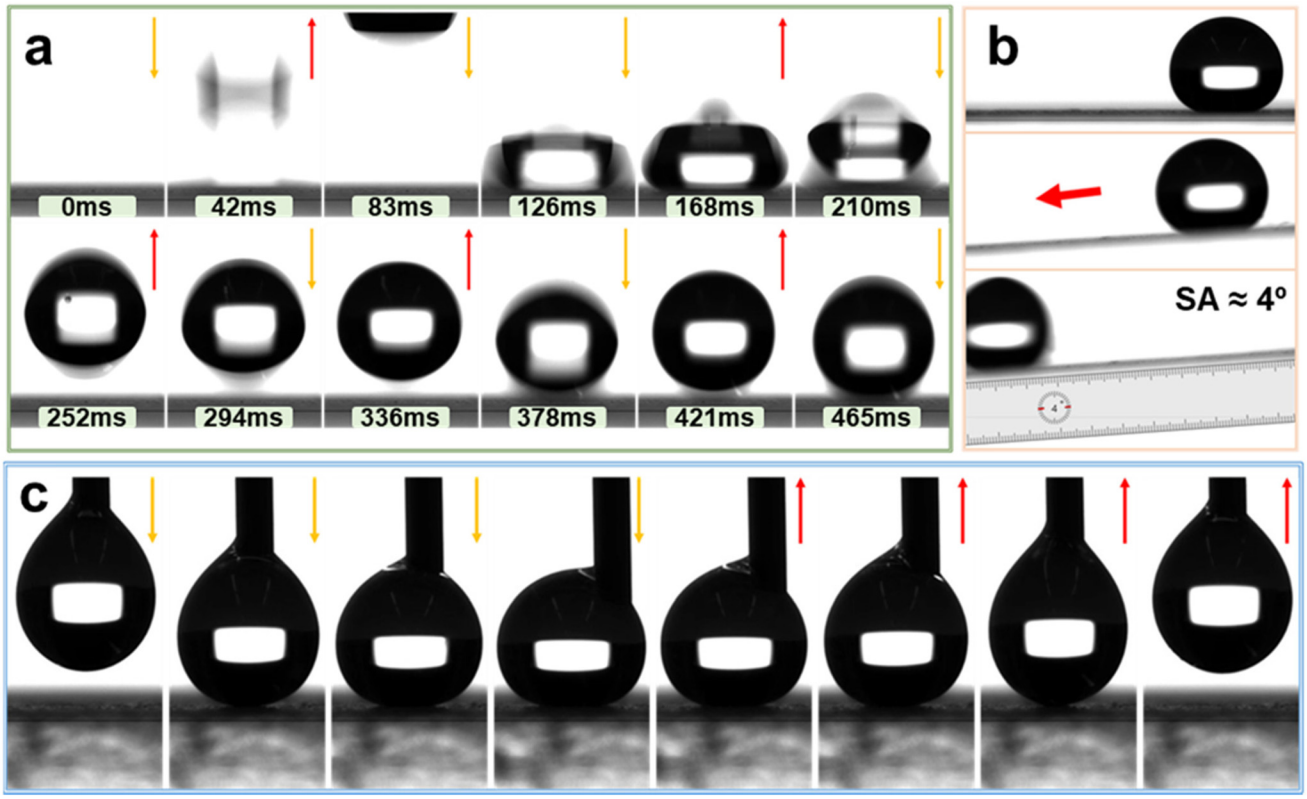

Fig. 7 Analysis of dynamic behaviour of water droplets. (a) Images demonstrate the repeating bounce behavior of a 15 μL water droplet on a horizontally placed spray-coated glass. (b) The SA test result of AFSR/EP@n-SiO_2 coatings with a 15 μL water droplet. (c) The test process of non-stacking property of AFSR/EP@n-SiO_2 coatings towards the water droplet using a contact angle measuring instrument.

ately after the first impact on the superhydrophobic surface at around 42 ms. The kinetic energy is dissipated by the internal viscous resistance of the droplet due to adhesion forces, and the energy loss of the droplet gradually increases over time, resulting in a decrease in the height of the droplet rebound after each impact. Until the kinetic energy is completely dissipated, the droplet comes to a stop on the surface. During the 465 ms dynamic process, the droplet rapidly spreads in all directions under the influence of inertia until it reaches the maximum spreading state and compresses into a pancake shape. Then, under the action of capillary forces, the droplet begins to restore its complete spherical shape and exhibits five complete bouncing behaviour on the surface.[62] As shown in Fig. 7b and Movie S3 of the ESI,† with the tilt angle of the coating sample gradually increasing, the SA of the droplet on the AFSR/EP@n-SiO_2 coating after the impact test decreases to

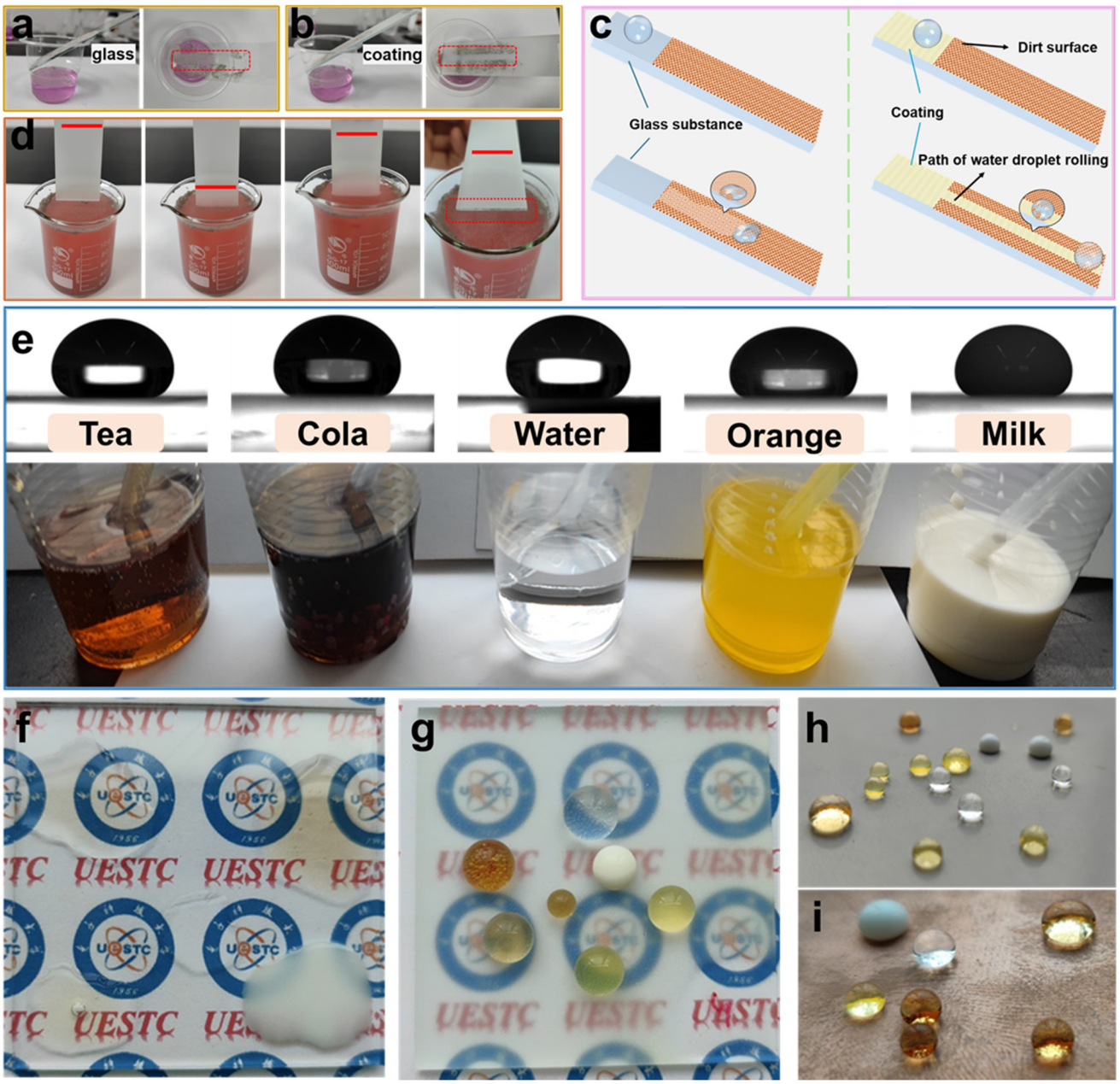

Fig. 8 Digital images demonstrating the self-cleaning ability of deposited dirt particles on both (a) uncoated and (b) coated glass sheets. (c) Self-cleaning process diagram and self-cleaning mechanism of uncoated and coated glass sheets. (d) Self-cleaning test of AFSR/EP@n-SiO_2 superhydrophobic coating by immersing in the muddy water. (e) Static contact angle images on coated samples using approximately 50 μL of various solutions and corresponding optical photographs. Optical photograph of solutions on (f) uncoated and (g) coated glass sheets. Optical photograph of different solutions on coated (h) steel sheet and (i) copper-clad plate.

~4°, indicating that the droplet easily rolls on the AFSR/EP@n-SiO_2 coating surface.

Further insight into the adhesion between water droplets and the prepared superhydrophobic coating was gained by placing a 10 μL water droplet on the coating surface from a syringe and observing its dynamic adhesion process. Fig. 7c and Movie S4 of the ESI† show the process of the water droplet approaching, contacting, squeezing, lifting, and leaving the coating surface. As the syringe slowly approached the coating surface, the water droplet was deformed, and the center of the syringe was offset on the coating surface. Once the syringe was lifted, the water droplet would completely leave the coating surface without any residue. This indicates that the synergistic effect of the unique surface structure constructed by the nanoparticles and the low surface energy AFSR greatly enhance the non-adhesive performance of the coating to water droplets. The above experimental results demonstrate that the adhesion of AFSR/EP@n-SiO_2 coating to water is small, enabling droplets to quickly leave the material surface, which is of great significance for the application of superhydrophobic coatings in areas such as anti-icing, self-cleaning, and droplet condensation.

3.6. Self-cleaning and anti-fouling performance

Self-cleaning performance is one of the important properties of superhydrophobic coatings in practical applications.[18,32,51] Due to the stronger adhesion of dust particles to water droplets, when water droplets roll off the superhydrophobic surface, dust particles are carried away by the water droplets to achieve the effect of automatic surface cleaning. In this experiment, self-cleaning tests were conducted by dropping water droplets on the AFSR/EP@n-SiO_2 superhydrophobic coating with a dust layer and immersing the samples in polluted water to evaluate their self-cleaning performance. The self-cleaning test on bare glass (Fig. 8a) showed clear traces of water droplet spreading and a failure to remove pollutants, indicating inferior self-cleaning performance of bare glass. This is because the exposed glass surface has a large number of hydrophilic hydroxyl groups, which make the surface have a strong affinity with water, and the water droplets spreading on the glass surface cannot achieve the self-cleaning effect, as shown in the schematic diagram of self-cleaning effect in Fig. 8c. In contrast, as shown in Fig. 8b and c, when the water droplet was dropped on the coated glass, the water droplet quickly rolled and left the coating surface, forming a straight clean path without dust. This result indicates that the pollutants on the coating can be easily carried away by water droplets, demonstrating the excellent self-cleaning performance of the AFSR/EP@n-SiO_2 coating. As shown in Fig. 8d, the sample coated with AFSR/EP@n-SiO_2 was repeatedly soaked in dyeing wastewater and pulled out after stirring. The coating surface was kept clean without being wetted by the wastewater, while obvious stains were attached to the uncoated area at the bottom of the sample. Then, the polluted water was repeatedly dropped on the coating, and the coating remained clean, which further confirms the splendid self-cleaning performance of AFSR/EP@n-SiO_2 coating. (Videos of self-cleaning performance tests of AFSR/EP@n-SiO_2 superhydrophobic coatings are displayed in movies S5 and S6 of the ESI.†) Fig. 8e shows the images and static contact angle images (droplets are added *via* a dropper and have a volume of about 50 μL) of common liquids. The AFSR/EP@n-SiO_2 coating showed good resistance to tea, cola, water, orange juice, and milk drops. Compared with the spreading state of droplets on the bare glass surface (Fig. 8f), droplets on the coated glass sample showed a more spherical shape (Fig. 8g). In addition to glass, the coating can be applied to surfaces of various substrates using the same method. The superhydrophobic coatings were sprayed on steel plates and copper-clad boards (Fig. 8h and i), and various liquid droplets exhibited excellent water repellency on the substrate surface. It is worth noting that the coating samples on cardboard substrate also showed an excellent water-repellent effect at room temperature for 24 h (Fig. S10 in the ESI†), indicating that the superhydrophobic sol prepared by spray method can be easily and widely applied to surface hydrophobic modification of various substrates.

4. Conclusions

In summary, by utilizing a two-step spray coating strategy, we have successfully designed and developed a silicone/epoxy resin superhydrophobic dual-layer composite coating. The amino fluorine-silicone resin not only enhances its own adhesive capabilities by being fully compatible with the epoxy resin through amine–epoxy "click" chemical reaction but also provides the necessary low surface energy conditions for the hydrophobicity of the coating. The incorporation of n-SiO_2 further enhances the micro-nano structural morphology of the coating surface, greatly improving its hydrophobic properties. Combining the dual advantages of the high stability of the silicone resin with the strong adhesive capabilities of the epoxy resin, the coating exhibits excellent wear resistance, resistance to physical and chemical environmental damage, as well as outstanding adhesion to substrates. The prepared AFSR/EP@SiO_2 coating can withstand strong acid and alkali immersion for 24 h, 1000-grit sandpaper moving 250 cm under a pressure of 200 g, scratches from sharp knives, immersion in 10 wt% NaCl solution for 48 h, and 30 W UV radiation for 32 days, while still maintaining superhydrophobic properties. The n-SiO_2 and AFSR/EP form a micro/nano rough mesh structure through spray coating, which provides and locks a large amount of air to form air pockets, allowing the droplets on the surface of the coating to be in a Cassie–Baxter state, thereby exhibiting excellent superhydrophobic properties (contact angle > 160°, rolling angle < 4°) and outstanding self-cleaning performance for liquid and solid pollutants. This design strategy and preparation process not only provide new ideas for the preparation of simple and easy-to-use superhydrophobic coatings but also expand the development and application of silicone resin in the fields of cleanliness and protection, such as photovoltaic solar energy, light-emitting diode panels, glass curtain walls, and electronic circuits.

Author contributions

Weidong Huang: data curation, formal analysis, methodology, investigation, writing original draft, writing – review and editing. Xiaoli Jiang: data curation, writing original draft, writing – review and editing. Yagang Zhang: conceptualization, writing – original draft, methodology, investigation, formal analysis, funding acquisition, project administration, writing – review and editing. Zhiqiang Tang: data curation, formal analysis. Zicai Sun: funding acquisition, project administration, writing – review and editing. Zhijun Liu: data curation, formal analysis. Lin Zhao: data curation, formal analysis, methodology. Yanxia Liu: measurement supervision, formal analysis. All authors have read and agree to the published version of the manuscript.

Conflicts of interest

There are no conflicts to declare.

Acknowledgements

This research was financially supported by the Key Research and Development Projects of Sichuan Province (2023YFG0222), Dongguan Introduction Program of Leading Innovative and Entrepreneurial Talents (20191122), "Tianfu Emei" Science and Technology Innovation Leader Program in Sichuan Province (2021), University of Electronic Science and Technology of China Talent Start-up Funds (A1098 5310 2360 1208), and National Natural Science Foundation of China (21464015, 21472235).

References

1 W. Li, Y. Shi, Z. Chen and S. Fan, *Nat. Commun.*, 2018, **9**, 4240.
2 B. A. Rorem, T. H. Cho, N. Farjam, J. D. Lenef, K. Barton, N. P. Dasgupta and L. J. Guo, *ACS Appl. Mater. Interfaces*, 2022, **14**, 31099–31108.
3 F. Shahzad, M. Alhabeb, C. B. Hatter, B. Anasori, S. M. Hong, C. M. Koo and Y. Gogotsi, *Science*, 2016, **353**, 1137–1140.
4 Z. Li, X. Chao, A. Balilonda and W. Chen, *InfoMat*, 2023, **5**, e12418.
5 C. Su, L. Zhou, C. Yuan, X. Wang, Q. Zhao, X. Zhao and G. Ju, *Compos. Sci. Technol.*, 2023, **231**, 109785.
6 T. Zhu, Y. Cheng, J. Huang, J. Xiong, M. Ge, J. Mao, Z. Liu, X. Dong, Z. Chen and Y. Lai, *Chem. Eng. J.*, 2020, **399**, 125746.
7 C. Cao, B. Yi, J. Zhang, C. Hou, Z. Wang, G. Lu, X. Huang and X. Yao, *Chem. Eng. J.*, 2020, **392**, 124834.
8 Y. Liu, X. Tan, X. Li, T. Xiao, L. Jiang, S. Nie, J. Song and X. Chen, *Langmuir*, 2022, **38**, 12881–12893.
9 W. H. Pan, Q. L. Wang, J. Ma, W. Xu, J. Sun, X. Liu and J. L. Song, *Adv. Funct. Mater.*, 2023, **33**, 2302311.
10 H. Zheng, Y. Chen, S. He, W. Liu, N. Liu, R. Guo and Z. Mo, *Colloids Surf., A*, 2023, **660**, 130856.
11 W. He, F. Zhang, F. Zhang and Q. He, *J. Appl. Polym. Sci.*, 2023, **140**, e53274.
12 B. Xie, Z. Chen, L. Ying, F. Huang and Y. Cao, *InfoMat*, 2020, **2**, 57–91.
13 L. Feng, S. Li, Y. Li, H. Li, L. Zhang, J. Zhai, Y. Song, B. Liu, L. Jiang and D. Zhu, *Adv. Mater.*, 2002, **14**, 1857–1860.
14 Y. Qing, C. Yang, N. Yu, Y. Shang, Y. Sun, L. Wang and C. Liu, *Chem. Eng. J.*, 2016, **290**, 37–44.
15 P. Velez-Herrera, K. Doyama, H. Abe and H. Ishida, *Macromolecules*, 2008, **41**, 9704–9714.
16 D. O'Hagan, *Chem. Soc. Rev.*, 2008, **37**, 308–319.
17 T. S. Wong, S. H. Kang, S. K. Y. Tang, E. J. Smythe, B. D. Hatton, A. Grinthal and J. Aizenberg, *Nature*, 2011, **477**, 443–447.
18 Y. Cao, H. P. Wu, S. I. Allec, B. M. Wong, D. S. Nguyen and C. Wang, *Adv. Mater.*, 2018, **30**, 1804602.
19 M. Guerre, C. Taplan, R. Nicolay, J. M. Winne and F. E. Du Prez, *J. Am. Chem. Soc.*, 2018, **140**, 13272–13284.
20 K. R. Carter, R. A. DiPietro, M. I. Sanchez and S. A. Swanson, *Chem. Mater.*, 2001, **13**, 213–221.
21 M. Liu, Z. Wang, P. Liu, Z. Wang, H. Yao and X. Yao, *Sci. Adv.*, 2019, **5**, 5643.
22 F. Sun, Y. Hu and H.-G. Du, *J. Appl. Polym. Sci.*, 2012, **125**, 3532–3536.
23 D. Zhuo, A. Gu, G. Liang, J.-T. Hu, L. Yuan and X. Chen, *J. Mater. Chem. A*, 2011, **21**, 6584–6594.
24 S. M. A. Mousavi and R. Pitchumani, *Corros. Sci.*, 2021, **186**, 109420.
25 X. Bai, S. Yang, C. Tan, T. Jia, L. Guo, W. Song, M. Jian, X. Zhang, Z. Zhang, L. Wu, H. Yang, H. Li and D. Hao, *J. Cleaner Prod.*, 2022, **380**, 134975.
26 J. Pi, C.-B. Li, R.-Y. Sun, L.-Y. Li, F. Wang, F. Song, J.-M. Wu, X.-L. Wang and Y.-Z. Wang, *Composants Commun.*, 2022, **32**, 101167.
27 D. Ebert and B. Bhushan, *J. Colloid Interface Sci.*, 2016, **481**, 82–90.
28 A. Allahdini, R. Jafari and G. Momen, *Prog. Org. Coat.*, 2022, **165**, 106758.
29 H. Zheng, W. Liu, S. He, R. Wang, J. Zhu, X. Guo, N. Liu, R. Guo and Z. Mo, *Colloids Surf., A*, 2022, **648**, 129152.
30 Y. Li, L. Li, D. Wan, A. Sha, Y. Li and Z. Liu, *Constr. Build. Mater.*, 2022, **360**, 129478.
31 S. M. Son, M. Kim, J. J. Yoo, M. S. Kim, B.-S. Kim and D. G. Seong, *Compos. Sci. Technol.*, 2023, **238**, 110048.
32 Q. Wang, G. Sun, Q. Tong, W. Yang and W. Hao, *Chem. Eng. J.*, 2021, **426**, 130829.
33 M. Yu, C. Fan, S. Han, F. Ge, Z. Cui, Q. Lu and X. Wang, *Prog. Org. Coat.*, 2020, **147**, 105867.
34 X. Zhao, D. S. Park, J. Choi, S. Park, S. A. Soper and M. C. Murphy, *J. Colloid Interface Sci.*, 2020, **574**, 347–354.
35 X. Y. Huang, C. Y. Zhi, P. K. Jiang, D. Golberg, Y. Bando and T. Tanaka, *Adv. Funct. Mater.*, 2013, **23**, 1824–1831.

36 Y. P. Mamunya, V. V. Davydenko, P. Pissis and E. Lebedev, *Eur. Polym. J.*, 2002, **38**, 1887–1897.
37 E. Ozeren Ozgul and M. H. Ozkul, *Constr. Build. Mater.*, 2018, **158**, 369–377.
38 Y. Wang, S. Chen, X. Chen, Y. Lu, M. Miao and D. Zhang, *Composites, Part B*, 2019, **160**, 615–625.
39 A. E. Krauklis and A. T. Echtermeyer, *Polymers*, 2018, **10**, 1017.
40 M. Shon and H. Kwon, *Corros. Sci.*, 2009, **51**, 650–657.
41 Z. Tang, Y. Liu, Y. Zhang, Z. Sun, W. Huang, Z. Chen, X. Jiang and L. Zhao, *Nanomaterials*, 2023, **13**, 1137.
42 C. Wang, L. Luo and H. Yamamoto, *Acc. Chem. Res.*, 2016, **49**, 193–204.
43 R. Wang, M. Sun, C. Wang, A. Dong and J. Zhang, *J. Polym. Sci.*, 2023, **61**, 223–233.
44 H. Gao, M. M. Wang, Y. F. Mao, Q. S. Zhao, C. Zhang, L. Jin, Y. Y. Xia, W. J. Li, K. Zhang and H. B. Zeng, *Adv. Mater.*, 2023, **35**, 202300616.
45 Y. Sun, H. He, X. Huang and Z. Guo, *ACS Appl. Mater. Interfaces*, 2023, **15**, 01998–04813.
46 F. Gao, L. A. Song, Z. M. Tong, T. J. Gui, W. W. Cong, K. Zhang, X. R. Wu, Q. Liu, Y. Y. Ren, X. L. Zhan and Q. H. Zhang, *Chem. Eng. J.*, 2023, **455**, 139894.
47 H. Yu, M. Wu, G. Duan and X. Gong, *Nanoscale*, 2022, **14**, 1296–1309.
48 Z. Shi, H. Zeng, Y. Yuan, N. Shi, L. Wen, H. Rong, D. Zhu, L. Hu, L. Ji, L. Zhao and X. Zhang, *Adv. Funct. Mater.*, 2023, **33**, 2213042.
49 H. Chen, F. Wang, H. Fan, R. Hong and W. Li, *Chem. Eng. J.*, 2021, **408**, 127343.
50 R. Sukamanchi, D. Mathew and K. S. S. Kumar, *ACS Sustainable Chem. Eng.*, 2017, **5**, 252–260.
51 N. B. Nguyen, N. H. Ly, H. N. Tran, S. J. Son, S. W. Joo, Y. Vasseghian, S. M. Osman and R. Luque, *Small Methods*, 2023, **7**, 2201257.
52 R. Chen, Y. Zhang, Q. Xie, Z. Chen, C. Ma and G. Zhang, *Adv. Funct. Mater.*, 2021, **31**, 2011145.
53 Y. Shen, Z. Wu, J. Tao, Z. Jia, H. Chen, S. Liu, J. Jiang and Z. Wang, *ACS Appl. Mater. Interfaces*, 2020, **12**, 25484–25493.
54 R. Zhu, M. Liu, Y. Hou, L. Zhang, M. Li, D. Wang and S. Fu, *ACS Appl. Mater. Interfaces*, 2020, **12**, 17004–17017.
55 Z. Bao, M. Gao, Y. Sun, R. Nian and M. Xian, *Mater. Sci. Eng., C*, 2020, **111**, 110796.
56 Y. Song, Z. Wang, Y. Li and Z. Dai, *Friction*, 2022, **10**, 44–53.
57 P. Nepal, S. Kalapugama, M. Shevlin, J. R. Naber, L.-C. Campeau, C. Pezzetta, A. Carlone, C. J. Cobley and S. H. Bergens, *ACS Catal.*, 2022, **12**, 2034–2044.
58 Y. Lu, X. Xu and J. Li, *J. Mater. Chem. B*, 2023, **11**, 3338–3355.
59 R. S. Sutar, P. J. Kalel, S. S. Latthe, D. A. Kumbhar, S. S. Mahajan, P. P. Chikode, S. S. Patil, S. S. Kadam, V. H. Gaikwad, A. K. Bhosale, K. K. Sadasivuni, S. Liu and R. Xing, *Macromol. Symp.*, 2020, **393**, 2000034.
60 X. Gao and Z. Guo, *J. Colloid Interface Sci.*, 2018, **512**, 239–248.
61 M. Luo, X. Sun, Y. Zheng, X. Cui, W. Ma, S. Han, L. Zhou and X. Wei, *Appl. Surf. Sci.*, 2023, **609**, 155299.
62 J. Zhang, L. Zhang and X. Gong, *Langmuir*, 2021, **37**, 6042–6051.
63 Y. He, L. Wang, T. Wu, Z. Wu, Y. Chen and K. Yin, *Nanoscale*, 2022, **14**, 9392–9400.
64 W. Luo, J. Xu, G. Li, G. Niu, K. W. Ng, F. Wang and M. Li, *Langmuir*, 2022, **38**, 7129–7136.
65 J. Zhao, S. Chen, W. Su, L. Zhu, X. Cheng, J. Wu, S. Zhao and C. Zhou, *Thin Solid Films*, 2021, **717**, 138467.
66 J. Huang, M. Yang, H. Zhang and J. Zhu, *ACS Appl. Mater. Interfaces*, 2021, **13**, 1323–1332.
67 Z. Ji, Y. Liu and F. Du, *Prog. Org. Coat.*, 2021, **157**, 106294.